

Article

Research on Energy Loss Characteristics of Pump-Turbine during Abnormal Shutdown

Yuxuan Deng *, Jing Xu, Yanna Li, Yanli Zhang and Chunyan Kuang

BaiLie School of Petroleum Engineering, Lanzhou City University, Lanzhou 730071, China

* Correspondence: dengyuxuan@lzcw.edu.cn; Tel.: +86-159-0815-5884

Abstract: Pumped-storage hydropower (PSH) stations are an efficient emission-free technology to balance renewable energy generation instabilities. The pump-turbine is a core component of PSH stations requiring frequent start-up, shutdown, and working conditions for regulation tasks, making it prone to instabilities. Based on entropy production theory and vortex dynamics, we analyzed the energy loss characteristics for three working conditions of the pump, pump brake, and turbine when shutting down the pump-turbine. The results showed that the entropy production and vorticity of the spiral casing and draft tube remain almost constant, while the entropy production and vorticity of the runner region substantially change from the late pump braking to the late turbine condition. The entropy production and vorticity are derived from the guide vane transitioning to the runner flow channel through the vaneless space. The change law of energy loss through entropy production agrees with the change law of internal flow turbulence through vorticity. The entropy production analysis can quantify the energy loss and mark its location, while the vorticity analysis can quantify the degree of flow disturbance and show its location. The entropy production theory and vortex dynamics combination provide insights into the connection between undesirable flow phenomena and energy loss.

Keywords: pump-turbine; entropy production; vorticity; energy loss; numerical simulation



Citation: Deng, Y.; Xu, J.; Li, Y.; Zhang, Y.; Kuang, C. Research on Energy Loss Characteristics of Pump-Turbine during Abnormal Shutdown. *Processes* **2022**, *10*, 1628. <https://doi.org/10.3390/pr10081628>

Academic Editors: Santiago Lain and Omar Dario Lopez Mejia

Received: 28 July 2022

Accepted: 8 August 2022

Published: 17 August 2022

Publisher's Note: MDPI stays neutral with regard to jurisdictional claims in published maps and institutional affiliations.



Copyright: © 2022 by the authors. Licensee MDPI, Basel, Switzerland. This article is an open access article distributed under the terms and conditions of the Creative Commons Attribution (CC BY) license (<https://creativecommons.org/licenses/by/4.0/>).

1. Introduction

With the increasing proportion of renewable energy generation, deploying the peaking power of the corresponding scale is necessary to improve the safety and flexibility of the system operation [1]. Pumped storage hydropower (PSH) stations, which mainly undertake the tasks of peak and valley regulation and frequency and phase regulation, have been vigorously developed with their unique static and dynamic benefits. Therefore, they are practical and indispensable regulation tools for power systems with good development prospects [2,3].

As the “heart” of a PSH station, the pump-turbine must be started and shut down frequently according to different regulation tasks. Moreover, the operating conditions are changed frequently; thus, the unit passes through abnormal operating conditions, rapidly causing the vibration and efficiency reduction in the unit and endangering the safe and stable operation of the power station [4,5]. Liu et al. [6] introduced a reversible pump-turbine structure with S-shaped characteristics, which is essential for the transition process (start-up and load shedding). Yao et al. [7] combined the load shedding conditions of the Guangzhou PSH station under different guide vane closure laws and calculated the effect of guide vane closure laws. Walseth et al. [8] combined experiments and one-dimensional numerical calculations to study the pump-turbine flyaway process. Zhang et al. [9] used the VOF two-phase flow model to simulate the entire flow system numerically. The calculation results showed that the power station went through the pump, pump braking, and turbine conditions. Liu et al. [10,11] numerically simulated the transition process of the pump-turbine load dump and the pump-condition power failure shutdown. The

authors found that the pressure fluctuation in the region near the runner is large during the load dump, and the pressure inside the runner drops significantly when operating in the pump braking mode. Moreover, they found that the reverse flow in the spiral case and the stall phenomenon in the flow channel substantially affect the change in the water head. Mao et al. [12] improved the stability of the fluid inside the pump-turbine by reducing the pressure change rate and improving the flow pattern. In particular, a coordinated valve and guide vane adjustment was adopted during load shedding. The results showed that this synergistic regulation method was practical for the operational stability of the system, especially for the final load shedding stage. In-depth research was conducted by Xia et al. [13] on the phenomenon of violent pressure fluctuation and unstable runner load during the runaway process of the pump-turbine. The authors found that the amplitude of the low-frequency component of the axial force was proportional to the amplitude of the flow rate of change. Li et al. [14] used a dynamic grid to simulate the guide vane closure process, verified the changing trend performance based on steady-state experiments, and analyzed the change law of performance characteristics such as head, flow and torque, pressure, and speed during the guide vane closure process. Zhang et al. [15] found that the inter-blade vortex structure at the impeller inlet shifted to the forward vortex structure and the return vortex structure when the pump-turbine operates in the S-shaped region. Moreover, they found that the forward vortex structure mainly dropped frequency drop and introduced low-frequency pulsation. In contrast, the return vortex structure caused unstable fluctuations. Yang et al. [16] described the evolution of the flow pattern during the rapid change in the pump-turbine operating conditions and analyzed the mechanism of pressure pulsation change on the flow pattern transition. Yang et al. [17] selected four different pump-turbines to simulate the runaway process. The authors analyzed the similarities and differences between flow patterns and pressure fluctuations, indicating that the transient processes controlling the mechanism of flow pattern transition and pressure change is a crucial element in flow path design. Zhao et al. [18] studied the stability performance of PSH generation systems during the transition from condensing to generating mode, developed a mathematical model to describe this dynamic transition process, and effectively predicted the dynamic response of the system parameters. Finally, Yang et al. [19] studied the relationship between the pressure pulsation value in the center of the pump-turbine draft tube and the wall pressure pulsation value using the CFD method. The study provided the critical value of the wall pressure pulsation when cavitation occurred, providing a reference for determining the cavitation phenomenon using the wall pressure pulsation value in practical engineering.

Furthermore, hydraulic losses due to friction and unsteady flow in a pump-turbine degrade its efficiency. Gong et al. [20] applied the entropy production theory in the hydraulic analysis of a hydraulic turbine. The authors also performed three-dimensional steady-state flow simulations and entropy production calculations for a hydraulic turbine. The results showed that entropy production theory is applicable to evaluate the performance of a hydraulic turbine and has the advantage of determining the amount of energy dissipation and the location where dissipation occurs. Li et al. [21,22] proposed the wall equation and used entropy production theory to obtain the detailed distribution of hydraulic losses of the pump-turbine in the pump mode, calculated the hydraulic losses in the wall region, and compared the hydraulic losses calculated by entropy production and pressure difference. In this way, the authors obtained improved results. In particular, the entropy production theory was used to directly reflect the energy dissipation in the hump region of the pump-turbine. Fu et al. [23] analyzed the energy conversion process, loss distribution, and flow mechanism inside the pump-turbine based on the numerical simulation, using the combination of entropy production analysis and flow analysis. The results showed that the pump-turbine load shedding process was an energy dissipation process, and the energy was converted between various energy forms. Li et al. [24] optimized the design of the runner blade and guide vane of the bulb tubular turbine by applying the boundary vortex dynamics theory. The authors also analyzed the effect of the vortex on unit performance

and efficiency, and the results showed that the vortex distribution on the blade surface could effectively reflect the turbine performance. Li et al. [25] obtained the vortex dynamics parameters according to the vortex dynamics theory and analyzed the relationship between the vortex dynamics parameters and the hump characteristics. The results showed that the energy transfer between the flow channel and the fluid was performed through the vortex dynamics parameters, which is superior in evaluating the dynamic performance of the pump-turbine.

In summary, the traditional method of hydraulic loss analysis focuses on evaluating the pressure drop, which has some limitations and cannot determine precisely where the high hydraulic losses occur. However, entropy production theory and vortex dynamics analysis have strong practicality and accuracy in the energy loss in the pump-turbine transition process. Thus, to further verify the advantages of these two methods in the energy loss characteristics of pump-turbines, this study analyzes the energy loss characteristics of the pump-turbine shutdown process using entropy production and vorticity methods based on numerical simulation. In particular, the results of the two methods are compared to study their connection.

2. Numerical Model

2.1. Computational Method

In this study, the governing equations include the continuity equation of an incompressible fluid and the Reynolds-averaged Navier–Stokes (RANS) equation. The ANSYS CFX 17.0 commercial computational fluid dynamics software was used to solve the three-dimensional unsteady flow in a pump-turbine. In this study, the SST $k-\omega$ model is chosen as the turbulence model, considering the viscosity of the inner wall of the model compared with the standard $k-\epsilon$ model and the RNG $k-\epsilon$ model. This model has an improved turbulent shear stress transport, a more stable algorithm, and an improved simulation performance for the flow in narrow spaces [26].

For turbulent flow, the local entropy production is caused by the time-averaged motion and the pulsation velocity, which can be expressed as Equations (1) and (2), respectively.

$$\dot{S}_{\bar{D}}''' = 2\frac{\mu}{T} \left[\left(\frac{\partial \bar{\mu}_1}{\partial x_1} \right)^2 + \left(\frac{\partial \bar{\mu}_2}{\partial x_2} \right)^2 + \left(\frac{\partial \bar{\mu}_3}{\partial x_3} \right)^2 \right] + \frac{\mu}{T} \left[\begin{array}{l} \left(\frac{\partial \bar{\mu}_2}{\partial x_1} + \frac{\partial \bar{\mu}_1}{\partial x_2} \right)^2 + \left(\frac{\partial \bar{\mu}_3}{\partial x_1} + \frac{\partial \bar{\mu}_1}{\partial x_3} \right)^2 \\ + \left(\frac{\partial \bar{\mu}_2}{\partial x_3} + \frac{\partial \bar{\mu}_3}{\partial x_2} \right)^2 \end{array} \right], \quad (1)$$

$$\dot{S}'_D = \frac{\mu_{eff}}{T} \left\{ 2 \left[\begin{array}{l} \left(\frac{\partial \mu'_1}{\partial x_1} \right)^2 + \left(\frac{\partial \mu'_2}{\partial x_2} \right)^2 + \\ \left(\frac{\partial \mu'_3}{\partial x_3} \right)^2 \end{array} \right] + \begin{array}{l} \left(\frac{\partial \mu'_2}{\partial x_1} + \frac{\partial \mu'_1}{\partial x_2} \right)^2 + \left(\frac{\partial \mu'_3}{\partial x_1} + \frac{\partial \mu'_1}{\partial x_3} \right)^2 \\ + \left(\frac{\partial \mu'_2}{\partial x_3} + \frac{\partial \mu'_3}{\partial x_2} \right)^2 \end{array} \right\}, \quad (2)$$

where T is the temperature ($^{\circ}\text{C}$), and μ_{eff} is the effective dynamic viscosity of the fluid ($\text{Pa}\cdot\text{s}$).

In the Reynolds time-averaged algorithm, the entropy production caused by the pulsation velocity is unavailable. Thus, ω in the turbulence model is correlated with the entropy production generated by the pulsation velocity [27], which can be expressed as follows:

$$\dot{S}'_{D'} = \beta \frac{\rho \omega k}{T}, \quad (3)$$

where $\beta = 0.09$, ω is the turbulent vortex viscous frequency (s^{-1}), and k is the turbulent kinetic energy (m^2/s^2).

Then, the total local entropy production can be expressed as follows:

$$\dot{S}'''_D = \dot{S}'''_{\bar{D}} + \dot{S}'''_{D'}. \quad (4)$$

2.2. Computational Model

The main design parameters of the study object are as follows: nominal runner diameter $D = 349$ mm, the number of runner blades $Z_0 = 6$, the number of guide vane

$Z_1 = 28$, the number of stay vane $Z_2 = 14$, Table 1 summarizes the main technical parameters of a pump-turbine.

Table 1. Main technical parameters.

Parameter	Symbol	Unit	Value
Nominal diameter	D	mm	349
Number of runner blades	Z_0	(-)	6
Number of guide vanes	Z_1	(-)	28
Number of stay vanes	Z_2	(-)	14
Rated flow rate	Q_d	m^3/s	0.203
Optimal guide vane opening	α	$^\circ$	10
Optimal efficiency	E	%	92.61
Rated head	H	m	12

This study aims to investigate the energy loss characteristics of the pump-turbine when guide vane rejection occurs after a sudden power failure during pump operation. Thus, all the over-flow components of the entire pumped storage unit are considered the calculation domain, mainly including the spiral case, guide vane, stay vane, runner, and draft tube. UG NX software was used to model each different over-flow component in 3D, and the assembled full-flow channel calculation model is shown in Figure 1.

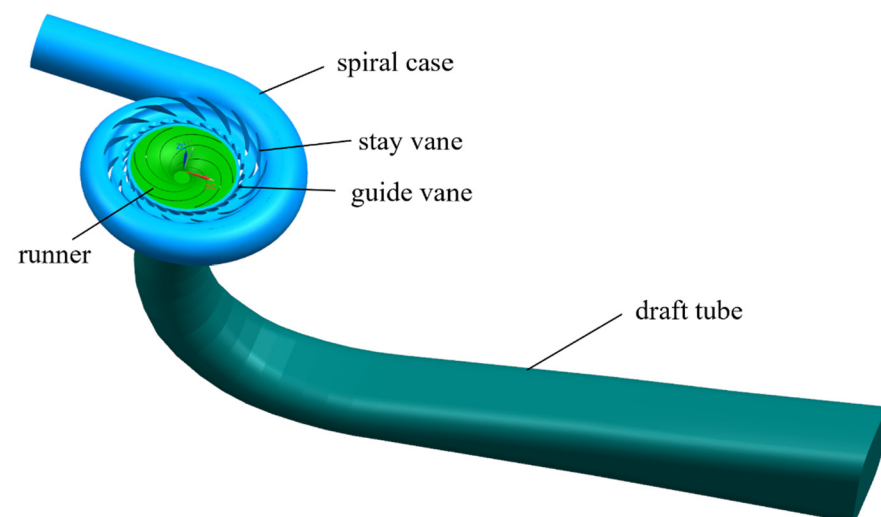


Figure 1. Computational model.

Considering the configuration of the computer (Intel Xeon E5-2650 @ 2.3 GHz with 64 GB of RAM) and the full-flow channel structure, this study was performed using the ICEM CFD commercial software because it required a high-precision structured grid for spatial discretization of the computational domain. For the components with narrow geometry, such as guide vanes and impellers, an “O-shaped” grid was used for the local encryption to ensure the uniform transition between the grids of each component and to capture the flow details accurately. The full flow channel and local grid are shown in Figure 2.

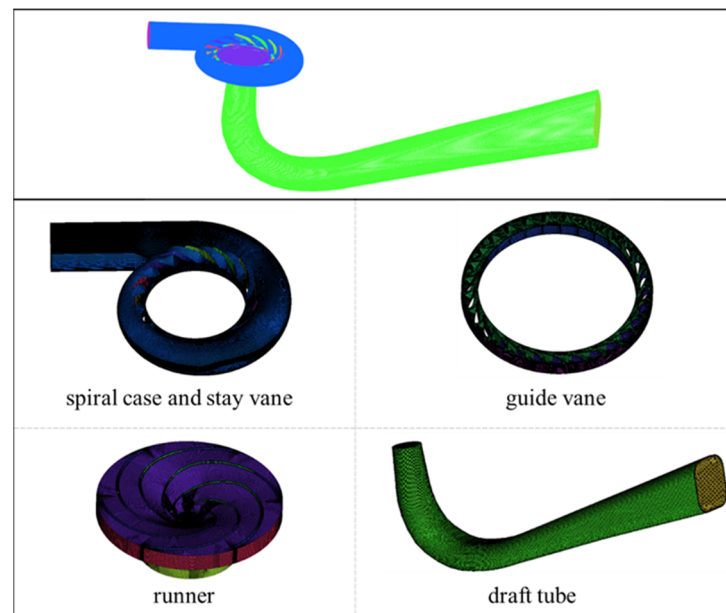


Figure 2. Computational mesh domain.

The grid density selected for the calculation should be as low as possible under the condition of satisfying the computational accuracy. In particular, the best efficiency point under the hydraulic turbine operating conditions should be selected for grid-independent analysis. The spiral case is the mass inlet boundary, which is set to $203 \text{ kg}\cdot\text{m}^3\cdot\text{s}^{-1}$, and the draft tube is the pressure outlet boundary, which is set to 111.13 kPa. The SST $k\text{-}\omega$ turbulence model was used, and the numerical solution of the control equations was obtained using the SIMPLEC algorithm for constant calculation. The residual convergence criterion was 10^{-5} . The quality of the grid was ensured using five sets of schemes with different grid numbers to validate and analyze with the head. The specific information of the grid is listed in Table 2, and the variation of the head with the number of grids is shown in Figure 3.

Table 2. Details of the grids.

Part	Nodes (Million)					Quality
	1	2	3	4	5	
Spiral case and Stay vane	1.58	2.05	3.78	4.82	8.36	0.30
Guide vane	0.76	0.94	1.09	1.83	2.48	0.42
Runner	2.11	2.11	2.11	2.11	2.11	0.33
Draft tube	0.75	1.00	1.41	1.89	2.70	0.38
Sum	5.20	6.10	8.40	10.65	15.65	—

As seen in Figure 3, the head variation is smooth when the number of grid nodes is greater than 8.4 million. Considering factors such as limited computational resources and computational time, the number of 8.4 million grid nodes was selected for numerical calculation.

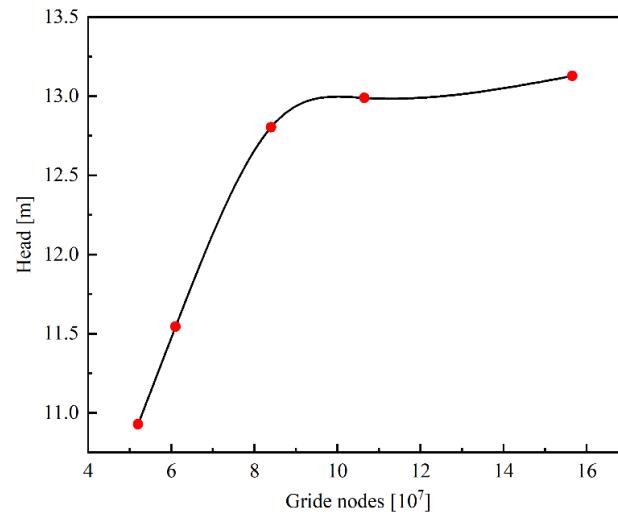


Figure 3. Grid independence verification.

2.3. Boundary Conditions and Setting

Figure 4 shows the N_{ed} - Q_{ed} characteristic curve of the pump-turbine in the transition process of guide vane rejection after the power failure in the pump condition. After the pump-turbine suddenly loses power in the pump condition, the flow rate decreases rapidly to zero along the pump condition direction. After entering the braking condition, the flow rate starts to increase in the reverse direction of the turbine condition, and the rotor speed starts to decrease rapidly to zero because the rotor blades lose power and are subject to fluid impact resistance. After entering the hydraulic turbine working condition, the runner starts to rotate to the hydraulic turbine working condition, and the impact of fluid on the runner blade provides power for the runner blade. The guide vane refuses to close the action, resulting in a continuous increase in rotational speed, and the unit finally enters the flyaway working condition area.

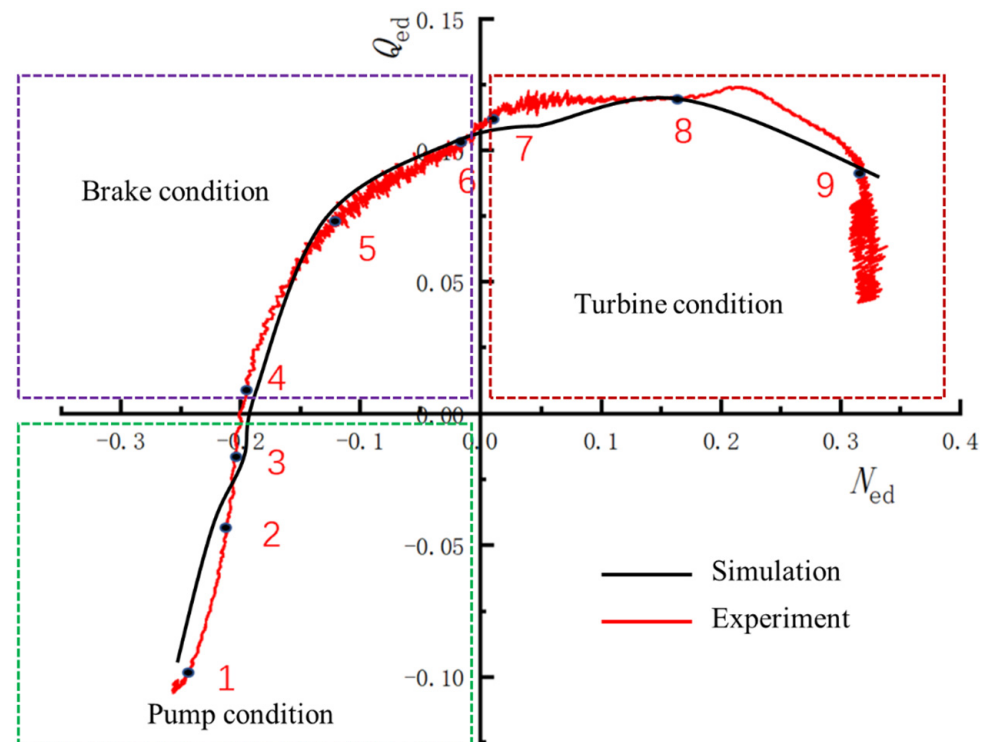


Figure 4. N_{ed} - Q_{ed} characteristic curve of pump-turbine.

In this study, nine working points in three working areas were selected for numerical simulation, and the numerical simulation, and experimental results were compared (where red is the curve obtained from the experiment and black is the curve obtained from the numerical simulation). As seen in Figure 4, the two characteristic curves basically match, indicating that the numerical simulation can reflect the flow characteristics of the pump-turbine during the power-off guide vane rejection transition.

The spiral case was selected as the mass flow inlet boundary condition, the flow direction was considered perpendicular to the inlet surface, and the turbulence intensity was 5%. The draft tube was used as the pressure outlet boundary condition, while the wall surface was used as the no-slip boundary condition. The runner speed was provided according to the experiment, and the connection between the spiral case, guide vane, runner, and draft tube was conducted using the interface. The numerical solution of the control equation was performed using the SIMPLEC algorithm. The transient calculation was performed using the constant calculation result as the non-constant initial field. The time step corresponded to the time of each 4° rotation of the runner, and the maximum iteration step was 80. The time step was the number of steps for ten rotations of the runner, which was set to 900. The calculated boundary conditions of each working condition are shown in Table 3.

Table 3. Boundary conditions.

Operating Point	Inlet(kPa)	Outlet (kPa)	Rotate Speed (rpm)	Turbulence Intensity	Time Step (s)
1	218.1	123.7	−461.7		−0.00014
2	193.7	125.5	−355.3		−0.00019
3	182.0	125.3	−319.0		−0.00021
4	181.5	125.3	−315.9		−0.00021
5	184.0	124.6	−211.9	5%	−0.00031
6	194.8	124.9	−18.8		−0.00355
7	190.8	124.9	16.6		0.00402
8	218.4	125.4	339.0		0.00020
9	229.3	126.6	600.2		0.00011

3. Results and Discussion

3.1. Energy Loss Analysis

When the water flows through the flow channel, the kinetic energy and pressure energy of the fluid are converted into internal energy due to the viscous force, increasing the entropy production. The energy losses can be obtained indirectly by analyzing the change in entropy production of each component during the pump-turbine shutdown. In particular, vorticity is one of the main causes of fluid energy loss in viscous fluid mechanics. Moreover, the flow disturbance phenomenon due to various irregular flows inside the pump-turbine can be quantified by vortex analysis. Therefore, the entropy production and vorticity change law of each component during the pump-turbine shutdown are compared and analyzed to study their connection.

Figure 5 shows the change curves of entropy production and vorticity of each component of the pump-turbine during the abnormal shutdown. As seen in the figure, the entropy production and vorticity of the spiral case and draft tube remain almost the same under different working conditions. In contrast, the entropy production and vorticity of the runner change substantially from the late stage of the pump braking condition to the late stage of the turbine working condition. The main reason is that under the pump braking condition, the internal fluid flows along the direction of the turbine, but the runner still rotates in the direction of the pump condition. The fluid flowing downstream through the guide vane is impacted by the blade, and a vortex is generated at the inlet of the runner and the pressure side of the runner blade head, resulting in energy loss. At the beginning of the turbine working condition, the runner rotates along the direction of the turbine working condition due to the impact of the fluid. At this time, the flow rate is large, the speed

is small, and the fluid impact loss is large. The following section focuses on the entropy production and vorticity of the runner part.

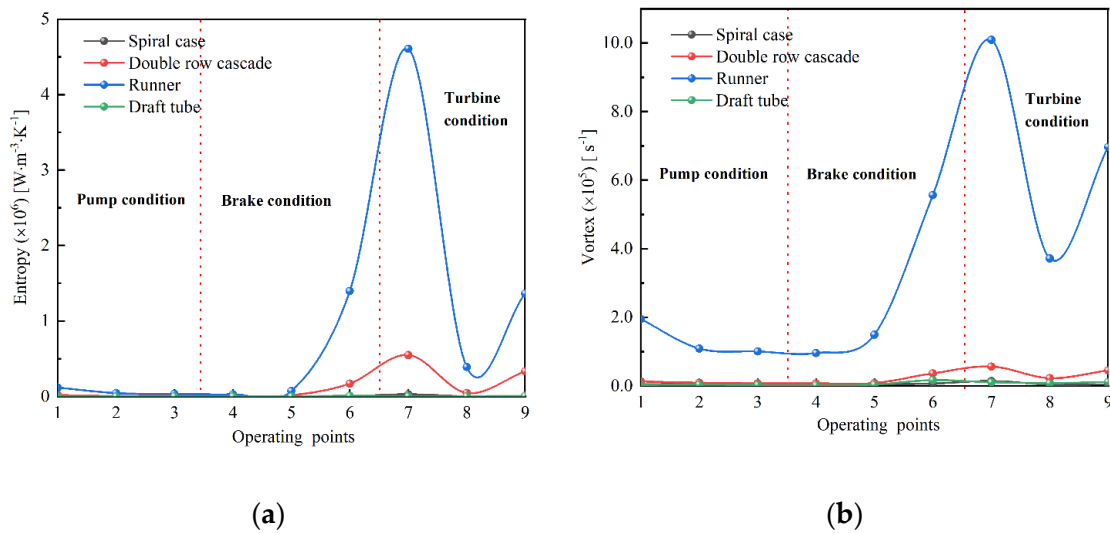


Figure 5. Energy loss during shutdown: (a) entropy production; (b) vorticity.

3.1.1. Entropy Production Analysis

Figure 6 shows the diagram of the entropy production distribution in the runner area under different working conditions. The diagram shows that the entropy production at the top of the runner blade is higher when the pump-turbine operates in the pump working condition. With the change in working condition point, the flow rate decreases, the fluid and blade impact weakens, and the entropy production reduces. The main reason is that after the sudden power failure of the unit, the guide vane refuses to act, and the fluid flows out of the runner and collides with the guide vane, resulting in part of the fluid flowing to the downstream runner area and blade impact. With the continuous reduction in flow, the fluid inside the unit reverses flow and starts to flow in the direction of the turbine. Moreover, the unit enters the braking condition zone, at which point the fluid flowing downstream through the guide vane is impacted by the blade, and a vortex is generated at the inlet of the runner and the pressure side of the runner blade head. When the working condition point 5 is reached, the entropy production of the front part of the runner is not uniformly distributed, the entropy production of the middle part is higher, and the entropy production of the middle part of the blade pressure side is also higher. When the working condition point 6 is reached, the entropy production of the top area of the blade is higher, and the high entropy production area of the runner is extended from the suction side of the front of the blade to the suction side of the tail, and the entropy production of the local area at the end of the runner is larger. After the rotational speed decreases to zero along the pump direction, the runner starts to rotate in the reverse direction and gradually increases along the turbine direction to enter the turbine working condition zone. When the working condition point 7 is reached, the front end of the blade is surrounded by the high entropy production area, and it extends along the front section of the runner to the end section. When the working condition point 8 is reached, the entropy production of the top area of the blade is higher, and the entropy production of the suction side of the blade is slightly higher than that of the surrounding area. Finally, when the working condition point 9 is reached, the entropy production of the entire vaneless space is higher due to the phenomenon of circulating flow in the vaneless space, and the entropy production of the front of the pressure side and the tail of the suction side of the blade is also significantly higher than that in the surrounding area.

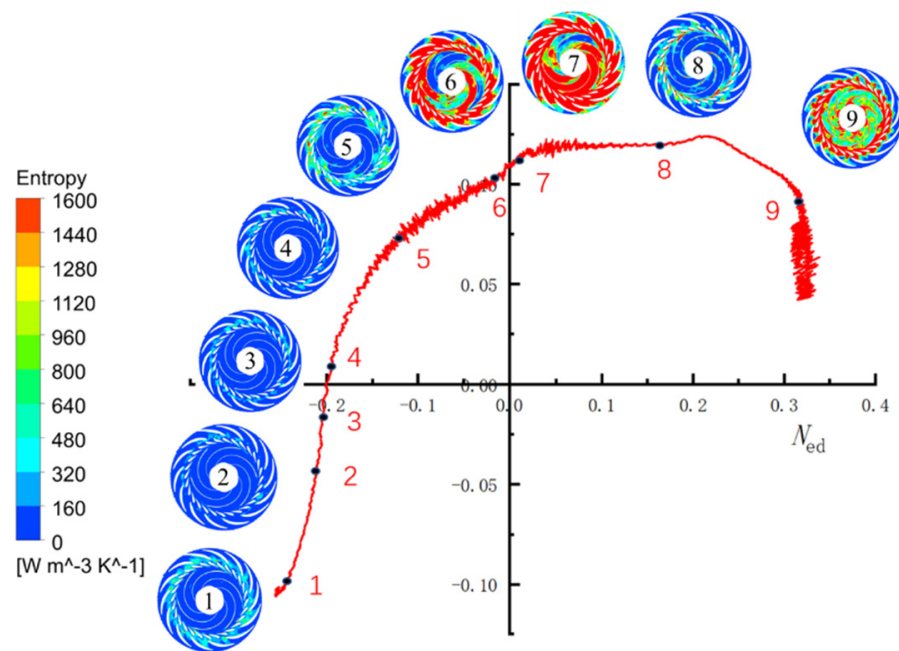


Figure 6. Diagram of the entropy production change in the runner area.

3.1.2. Vorticity Analysis

Figure 7 shows the vorticity distribution diagram in the runner area under different working conditions. The figure shows that the guide vane refuses to act after the sudden power failure, and the unit runs in the pump working condition area, the fluid flows out from the runner and collides with the guide vane, and part of the fluid flows to the downstream runner area and impacts with the blade. In this working condition zone, the vorticity at the top of the blade extends to the double-row impeller grille, and when it reaches the rear section of the blade, the pressure side vorticity becomes higher than that in the surrounding area. In the braking condition zone, the fluid flows in the direction of the turbine condition, and the runner rotates in the direction of the pump condition. When the working condition point 5 is reached, the vorticity on the pressure side of the blade head is substantially larger than that in the surrounding area. In particular, the vorticity distribution in the runner area is extremely uneven and gradually decreases along the runner. As the speed decreases, the flow rate increases, and the role of the blade on the fluid decreases and reaches the working condition point 6. In this condition, the high vorticity area only exists at the top of the blade, and the vorticity is much larger than the surrounding area. Moreover, the vorticity in the vaneless space is obviously reduced, the vorticity in the runner area along the center of the runner to both ends of the runner blade is decreased, and the vorticity at the end of the runner is larger. In the hydraulic turbine working condition area, the region with higher vorticity at the blade tip presents a U-shaped distribution. The area is more concentrated than the previous one, and the vorticity in the runner is small in the middle and large on both sides. When the working condition point 8 is reached, the vorticity on the suction side of the blade tip is larger, and the vorticity on the suction side of the runner near the blade is larger than that in other regions. Finally, when the working condition point 9 is reached, the high vorticity area at the top of the blade develops to the pressure side. Furthermore, the vorticity at the inlet of the runner is irregularly distributed, the vorticity value at the end of the runner is larger, and a ring-shaped area with high vorticity is present in the vaneless space.

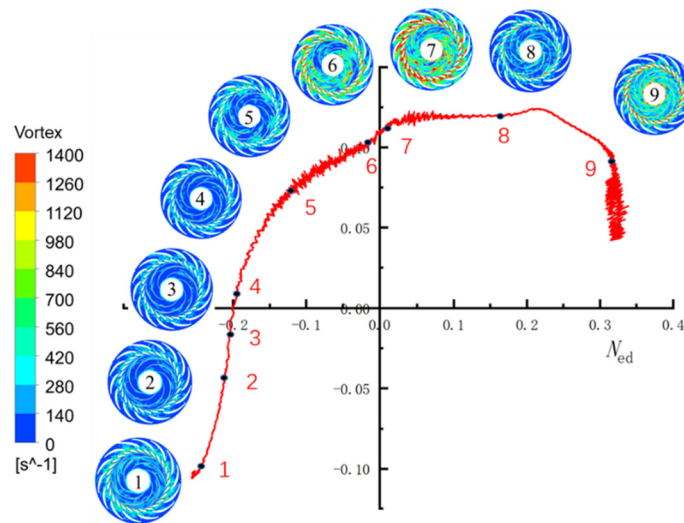


Figure 7. Diagram of the vorticity change in the runner area.

Figure 8 shows the curves of the entropy production and vorticity in the blade and double-row blade grille area during the abnormal shutdown of the pump-turbine. As seen in the figure, the entropy production and vorticity change trends are the same throughout the shutdown process. From the early stage of the pump condition to the middle of the braking condition, the entropy production and vorticity change slightly. Moreover, both curves rise rapidly from the middle of the braking condition, reaching the peak in the early stage of the turbine condition and decreasing rapidly. Subsequently, they rise rapidly after the middle of the turbine condition. The changing trend is consistent with the analysis results presented in Sections 3.1.1 and 3.1.2. Before the working condition point 5, the entropy production and vorticity slowly change. Then, they gradually increase from the working condition point 5 and reach the maximum value at the working condition point 7. Finally, both variables continue to rise to the working condition point 9 after dropping to the working condition point 8.

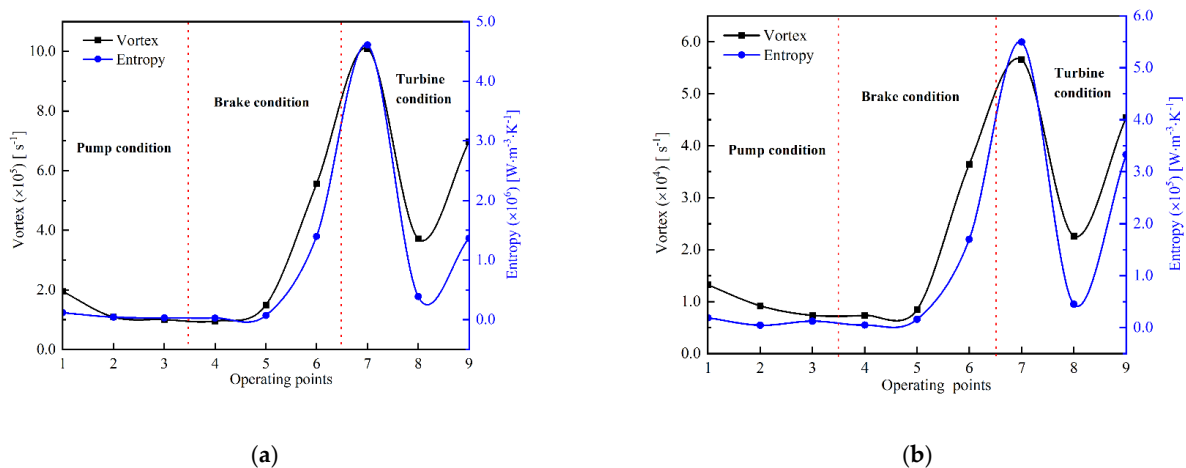


Figure 8. Comparison of the vorticity and entropy production: (a) blade; (b) double-row blade.

3.2. Distribution Law Analysis

The analysis presented above indicates that a certain correlation exists between the entropy production and vorticity of the pump-turbine in the process of the abnormal shutdown. In the following, the entropy production and vorticity of the runner area under the late braking condition, the pre-water turbine condition, and the late condition are analyzed to explore the internal flow mechanism of the distribution law of both.

Figure 9 shows the entropy production expansion diagram of the runner area under the three working conditions. As seen in the figure, most of the entropy production near the guide vane is high in the late braking condition. Only the entropy production at the head of the two guide vane in the A area is low, shown in the dashed box. Moreover, the distribution of entropy production in the bladeless space is chaotic; however, the overall intensity is high, and the entropy production starts from the guide vane and transitions to the impeller runners through the vaneless space. Nevertheless, in this condition, only the entropy production in the two runners is high and unevenly distributed. The remaining four runners have higher entropy production at the inlet or front end of the blade pressure side and have not started derived downstream. In the early stage of the turbine working condition, the entropy production in the guide vane area is uniformly distributed, and the intensity reaches the highest. The phenomenon of annular high entropy production in the vaneless region is enhanced, and only the entropy production in the B area shown in the dashed box is low. Moreover, the entropy production in the runner develops downstream, and the area of high entropy production in the entire runner increases significantly. The entropy production in two runners is high in intensity and uniformly distributed, while the entropy production in the rest is still in the transition process and disordered distributing. In the late stage of the turbine operation, the entropy production of the head of the movable guide vane (C area shown in the dashed box) exhibits a high and low intermittent distribution. The entropy production of the entire vaneless space to the front of the runner reaches the highest intensity and uniform distribution. In contrast, the entropy production of the middle part of the runner is low, and the entropy production of the pressure side of the rear part of the runner is high, with a regular overall distribution.

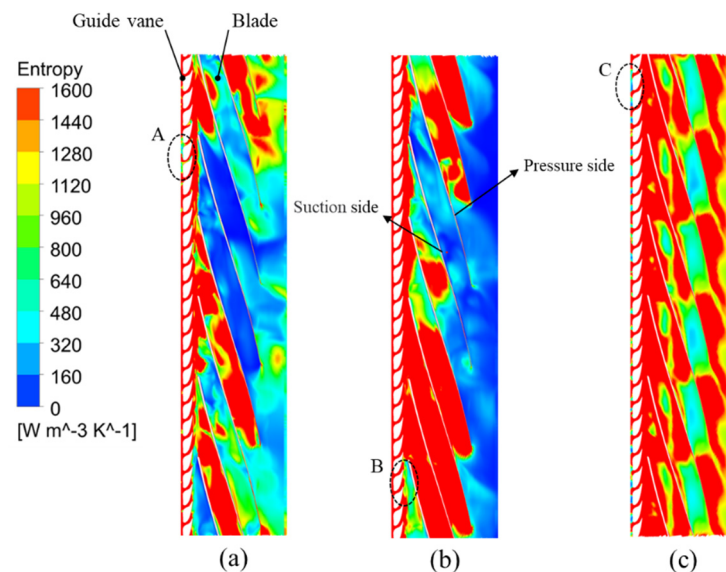


Figure 9. Distribution of the entropy production in the runner area: (a) late braking condition; (b) pre-water turbine condition; (c) late turbine operating condition.

Figure 10 shows the vortex diagram of the runner area under the three working conditions. Note that in the late braking condition, the middle and rear sections of the guide vane are all high vorticity areas, and some of them extend through the vaneless space to the head of the runner blade and occupy the pressure side flow channel entrance. Most of the blades have higher vorticity in the area near the pressure side front and middle section walls. Moreover, a small part of the blades has higher vorticity in the area near the suction side middle and rear section walls. Some of the blades have small-scale circular high vorticity areas at the end. In the early stage of the turbine working condition, the high vorticity area extends to the head of the guide vane, and the vorticity of the entire guide vane area is higher. Furthermore, the annular high vortex phenomenon in the vaneless space is enhanced, and the area of the high vorticity area of each part of the blade increases.

In the later stage of the turbine working condition, the vorticity near the head of the guide vane decreases, the high vorticity area only covers the middle and rear part of the guide vane, and the high vorticity area covers the vaneless space. The vorticity in the front and middle channels of the runner is higher on both sides of the blades and lower in the middle area. The vorticity in the middle area is low. Only a very small circular area in the rear part of the runner has high vorticity, and the overall distribution is more regular.

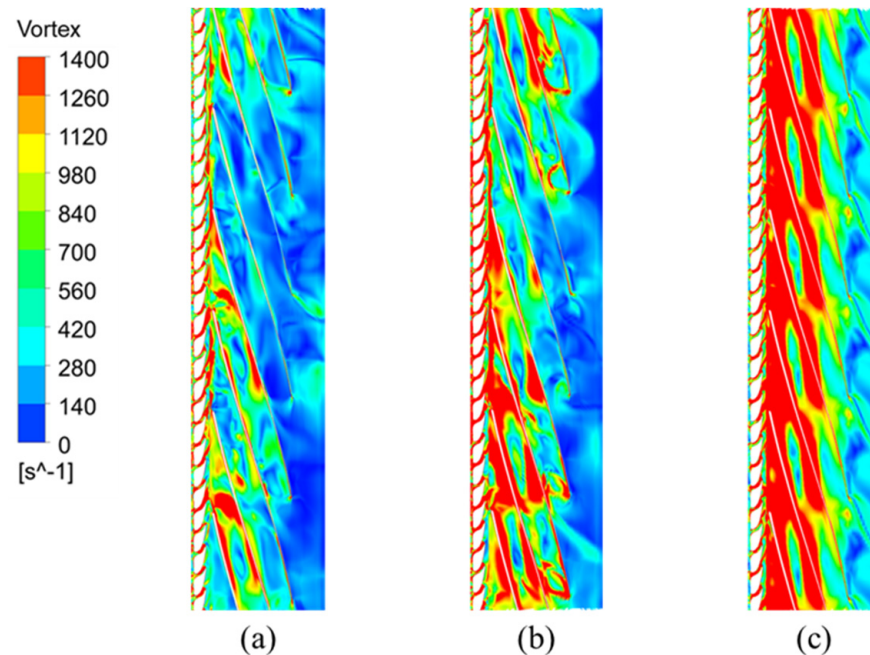


Figure 10. Vortex distribution in the runner area: (a) late braking condition; (b) pre-water turbine condition; (c) late turbine operating conditions.

Figure 11 shows the flow diagram of the pump-turbine in the runner area under different working conditions. Note that in the late braking condition, most of the guide vane head has swirling flow. In addition, the fluid flow velocity is larger near the pressure sidewall, and the high-speed circulation phenomenon appears at the tail wall of the guide vane pressure side. Almost all the runner channels are occupied by backflow and channel vortex, presenting a severe blockage. In the early stage of the hydraulic turbine working condition, the flow velocity increases, and the number of guide vortex decreases. Moreover, the high-speed circulation phenomenon in the vaneless space is weakened, and the number of vortex in the runner flow channel decreases. The fluid in part of the flow channel flows downstream at high speed along the suction sidewall of the blade. At the later stage of the turbine working condition, the number of swirling flows at the head of the guide vane increases, the scale increases, and the circulation phenomenon in the vaneless space becomes evident. Furthermore, the scale of the vortex in the runner flow channel becomes smaller, the number increases, and most of the swirling flows locate near the wall of the suction side of the runner blade. As the shutdown process proceeds, the swirling flow around the guide vane is produced easily due to the development of backflow. Moreover, the high-speed circulation phenomenon produces easily due to the vaneless space so that the fluid cannot smoothly flow downstream. In addition, in the runner backflow, off-flow and other phenomena developed from the vortex. Through the comparative analysis of the vorticity, entropy production, and flow line, the vorticity and entropy production distribution law is similar. In particular, the vorticity and the entropy production are larger in the parts with larger vortex flow or velocity gradient.

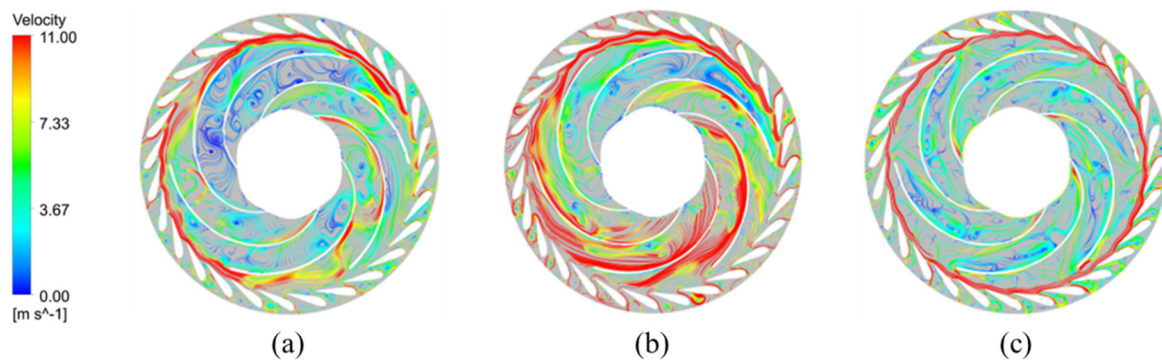


Figure 11. Flow diagram of the runner area: (a) late braking condition; (b) pre-water turbine condition; (c) late turbine operating conditions.

4. Conclusions

This study implemented the entropy production theory and vortex dynamics to study and analyze the energy loss characteristics in the process of pump-turbine shutdown. The following conclusions were obtained:

(1) During the abnormal shutdown of the pump-turbine, the entropy production, vorticity of the spiral case, and draft tube slightly changed. In contrast, the entropy production and vorticity of the runner area changed more drastically from the late braking condition to the late turbine condition, starting from the middle of the braking condition and rising rapidly to the peak in the early turbine condition and then decreasing rapidly. Subsequently, the entropy production and vorticity rise rapidly after the middle of the turbine condition.

(2) In the runner region, the entropy production and vorticity of the two distribution trends are similar. The head and tail of the movable guide vane rapidly produced the backflow phenomenon. Moreover, the vaneless area created a high-speed circulation phenomenon, the rotor blade wall near generated the leaf channel vortex. These irregular flow phenomena generated parts of the entropy production, with a high vorticity and energy loss.

(3) The analysis method using the combination of entropy production theory and vortex dynamics is practical. In particular, the entropy production analysis can quantify the energy loss and indicate the location of energy loss. Moreover, the vortex analysis can quantify the degree of flow disturbance and locate the flow disturbance, which can explore the connection between undesirable flow phenomena and energy loss.

Author Contributions: Conceptualization, Y.D.; methodology, Y.D.; writing—original draft preparation, J.X.; writing—review and editing, Y.L.; visualization, Y.Z.; supervision, Y.D.; software, C.K. All authors have read and agreed to the published version of the manuscript.

Funding: This research was funded by the Open Research Subject of Key Laboratory of Fluid and Power Machinery, Ministry of Education (Grant No. LTDL2020-005), Doctoral Research Foundation of Lanzhou City University (Grant No. LZCU-BS2019-07).

Institutional Review Board Statement: Not applicable.

Informed Consent Statement: Not applicable.

Data Availability Statement: All the data are already in the article.

Acknowledgments: The authors would like to thank all staff of the treatment plants for making.

Conflicts of Interest: The authors declare no conflict of interest.

References

1. Zhang, W.; Feng, D.; Qi, W.; Han, Z.; Guan, Y.; Sun, W.; Wang, W. Research on Peak Shaving Power Source Planning for Receiving-End Grid Considering High Proportion of New Energy and Large-Scale Outer Power. *IOP Conf. Ser. Earth Environ. Sci.* **2019**, *267*, 062009. [[CrossRef](#)]
2. Kong, Y.; Kong, Z.; Liu, Z.; Wei, C.; Zhang, J.; An, G. Pumped Storage Power Stations in China: The past, the Present, and the Future. *Renew. Sustain. Energy Rev.* **2017**, *71*, 720–731. [[CrossRef](#)]
3. He, Y.; Liu, Y.; Li, M.; Zhang, Y. Benefit Evaluation and Mechanism Design of Pumped Storage Plants under the Background of Power Market Reform—A Case Study of China. *Renew. Energy.* **2022**, *191*, 796–806. [[CrossRef](#)]
4. Kusakana, K. Optimal Scheduling for Distributed Hybrid System with Pumped Hydro Storage. *Energy Convers. Manag.* **2016**, *111*, 253–260. [[CrossRef](#)]
5. Yu, A.; Li, L.; Ji, J.; Tang, Q. Numerical Study on the Energy Evaluation Characteristics in a Pump Turbine Based on the Thermodynamic Entropy Theory. *Renew. Energy.* **2022**, *195*, 766–779. [[CrossRef](#)]
6. Liu, D.M.; Zheng, J.S.; Wen, G.Z.; Zhao, Y.Z.; Shi, Q.H. Numerical Simulation on the “S” Characteristics and Pressure Fluctuation of Reduced Pump-Turbine at Start-Up Condition. *IOP Conf. Ser. Earth Environ. Sci.* **2012**, *15*, 062034. [[CrossRef](#)]
7. Yao, Z.; Bi, H.L.; Huang, Q.S.; Li, Z.J.; Wang, Z.W. Analysis on Influence of Guide Vanes Closure Laws of Pump-Turbine on Load Rejection Transient Process. *IOP Conf. Ser. Mater. Sci. Eng.* **2013**, *52*, 072004. [[CrossRef](#)]
8. Walseth, E.; Nielsen, T.; Svingen, B. Measuring the Dynamic Characteristics of a Low Specific Speed Pump-Turbine Model. *Energies* **2016**, *9*, 199. [[CrossRef](#)]
9. Zhang, L.G.; Zhou, D.Q. CFD Research on Runaway Transient of Pumped Storage Power Station Caused by Pumping Power Failure. *IOP Conf. Ser. Mater. Sci. Eng.* **2013**, *52*, 052027. [[CrossRef](#)]
10. Jintao, L.; Shuhong, L.; Yuekun, S.; Yulin, W.; Leqin, W. Three Dimensional Flow Simulation of Load Rejection of a Prototype Pump-Turbine. *Eng. Comput.* **2013**, *29*, 417–426. [[CrossRef](#)]
11. Liu, J.; Liu, S.; Sun, Y.; Jiao, L.; Wu, Y.; Wang, L. Three-Dimensional Flow Simulation of Transient Power Interruption Process of a Prototype Pump-Turbine at Pump Mode. *J. Mech. Sci. Technol.* **2013**, *27*, 1305–1312. [[CrossRef](#)]
12. Mao, X.; Chen, X.; Lu, J.; Liu, P.; Zhang, Z. Improving Internal Fluid Stability of Pump Turbine in Load Rejection Process by Co-adjusting Inlet Valve and Guide Vane. *J. Energy Storage.* **2022**, *50*, 104623. [[CrossRef](#)]
13. Xia, L.; Cheng, Y.; Yang, Z.; You, J.; Yang, J.; Qian, Z. Evolutions of Pressure Fluctuations and Runner Loads during Runaway Processes of a Pump-Turbine. *J. Fluids Eng.* **2017**, *139*, 091101. [[CrossRef](#)]
14. Li, D.; Wang, H.; Li, Z.; Nielsen, T.K.; Goyal, R.; Wei, X.; Qin, D. Transient Characteristics during the Closure of Guide Vanes in a Pump-Turbine in Pump Mode. *Renew. Energy* **2018**, *118*, 973–983. [[CrossRef](#)]
15. Zhang, X.; Zeng, W.; Cheng, Y.; Yang, Z.; Chen, Q.; Yang, J. Mechanism of Fast Transition of Pressure Pulsations in the Vaneless Space of a Model Pump-Turbine during Runaway. *J. Fluids Eng.* **2019**, *141*, 121104. [[CrossRef](#)]
16. Yang, Z.; Cheng, Y.; Xia, L.; Meng, W.; Liu, K.; Zhang, X. Evolutions of Flow Patterns and Pressure Fluctuations in a Prototype Pump-Turbine during the Runaway Transient Process after Pump-Trip. *Renew. Energy* **2020**, *152*, 1149–1159. [[CrossRef](#)]
17. Yang, Z.; Liu, Z.; Cheng, Y.; Zhang, X.; Liu, K.; Xia, L. Differences of Flow Patterns and Pressure Pulsations in Four Prototype Pump-Turbines during Runaway Transient Processes. *Energies* **2020**, *13*, 5269. [[CrossRef](#)]
18. Zhao, Z.; Chen, D.; Li, H.; Wei, H. Performance Analysis of Pumped-Storage Plant from Condenser Mode to Generating Process. *J. Energy Storage* **2020**, *29*, 101286. [[CrossRef](#)]
19. Yang, J.; Lv, Y.; Liu, D.; Wang, Z. Pressure Analysis in the Draft Tube of a Pump-Turbine under Steady and Transient Conditions. *Energies* **2021**, *14*, 4732. [[CrossRef](#)]
20. Gong, R.; Wang, H.; Chen, L.; Li, D.; Zhang, H.; Wei, X. Application of Entropy Production Theory to Hydro-turbine Hydraulic Analysis. *Sci. China Technol. Sci.* **2013**, *56*, 1636–1643. [[CrossRef](#)]
21. Li, D.; Gong, R.; Wang, H.; Xiang, G.; Wei, X.; Qin, D. Entropy Production Analysis for Hump Characteristics of a Pump Turbine Model. *Chin. J. Mech. Eng.* **2016**, *29*, 803–812. [[CrossRef](#)]
22. Li, D.; Wang, H.; Qin, Y.; Han, L.; Wei, X.; Qin, D. Entropy Production Analysis of Hysteresis Characteristic of a Pump-Turbine Model. *Energy Convers. Manag.* **2017**, *149*, 175–191. [[CrossRef](#)]
23. Fu, X.; Li, D.; Wang, H.; Zhang, G.; Li, Z.; Wei, X.; Qin, D. Energy Analysis in a Pump-Turbine during the Load Rejection Process. *J. Fluids Eng.* **2018**, *140*, 101107. [[CrossRef](#)]
24. Li, F.; Fan, H.; Wang, Z.; Chen, N. Coupled Design and Optimization for Runner Blades of a Tubular Turbine Based on the Boundary Vorticity Dynamics Theory. In Proceedings of the Fluids Engineering Division Summer Meeting, Toronto, ON, Canada, 3–5 August 2022; pp. 603–609.
25. Li, D.; Gong, R.; Wang, H.; Han, L.; Wei, X.; Qin, D. Analysis of Vorticity Dynamics for Hump Characteristics of a Pump Turbine Model. *J. Mech. Sci. Technol.* **2016**, *30*, 3641–3650. [[CrossRef](#)]
26. Li, X.; Li, Z.; Zhu, B.; Wang, W. Effect of Tip Clearance Size on Tubular Turbine Leakage Characteristics. *Processes* **2021**, *9*, 1418. [[CrossRef](#)]
27. Kock, F.; Herwig, H. Local Entropy Production in Turbulent Shear Flows: A High-Reynolds Number Model with Wall Functions. *Int. J. Heat Mass Transf.* **2004**, *47*, 2205–2215. [[CrossRef](#)]